AMERICAN SOCIETY FOR MICROBIOLOGY | Antimicrobial Agents and Chemotherapy®

ANTIVIRAL AGENTS

Nitazoxanide Inhibits Human Norovirus Replication and Synergizes with Ribavirin by Activation of Cellular Antiviral Response

Wen Dang,[a] Lei Xu,[a] Buyun Ma,[a] Sunrui Chen,[a] Yuebang Yin,[a] Kyeong-Ok Chang,[b] Maikel P. Peppelenbosch,[a] Qiuwei Pan[a]

[a]Department of Gastroenterology and Hepatology, Erasmus MC-University Medical Center, Rotterdam, Netherlands

[b]Department of Diagnostic Medicine and Pathobiology, College of Veterinary Medicine, Kansas State University, Manhattan, Kansas, USA

ABSTRACT Norovirus is the main cause of viral gastroenteritis worldwide. Although norovirus gastroenteritis is self-limiting in immunocompetent individuals, chronic infections with debilitating and life-threatening complications occur in immunocompromised patients. Nitazoxanide (NTZ) has been used empirically in the clinic and has demonstrated effectiveness against norovirus gastroenteritis. In this study, we aimed at uncovering the antiviral potential and mechanisms of action of NTZ and its active metabolite, tizoxanide (TIZ), using a human norovirus (HuNV) replicon. NTZ and TIZ, collectively referred to as thiazolides (TZD), potently inhibited replication of HuNV and a norovirus surrogate, feline calicivirus. Mechanistic studies revealed that TZD activated cellular antiviral response and stimulated the expression of a subset of interferon-stimulated genes (ISGs), particularly interferon regulatory factor 1 (IRF-1), not only in a Huh7 cell-based HuNV replicon, but also in naive Huh7 and Caco-2 cells and novel human intestinal organoids. Overexpression of exogenous IRF-1 inhibited HuNV replication, whereas knockdown of IRF-1 largely attenuated the antiviral activity of TZD, suggesting that IRF-1 mediated TZD inhibition of HuNV. By using a Janus kinase (JAK) inhibitor, CP-690550, and a STAT1 knockout approach, we found that TZD induced antiviral response independently of the classical JAK-signal transducers and activators of transcription (JAK-STAT) pathway. Furthermore, TZD and ribavirin synergized to inhibit HuNV replication and completely depleted the replicons from host cells after long-term treatment. In summary, our results demonstrated that TZD combated HuNV replication through activation of cellular antiviral response, in particular by inducing a prominent antiviral effector, IRF-1. NTZ monotherapy or combination with ribavirin represent promising options for treating norovirus gastroenteritis, especially in immunocompromised patients.

KEYWORDS nitazoxanide, cell culture model, IRF-1, ribavirin, synergy, noroviruses, tizoxanide

Norovirus is one of the main causative agents of acute viral gastroenteritis in all age groups. It is estimated to cause a median of 699 million illnesses and 219,000 deaths every year, of which more than 90,000 deaths occur among children less than 5 years old (1). Currently, norovirus gastroenteritis is also recognized as an emerging burden in immunocompromised populations, particularly transplant recipients (2). Suppression of the immune system facilitates norovirus infection, resulting in chronic diarrhea and other complications (3, 4). Furthermore, norovirus gastroenteritis has been reported to cause graft versus host disease (GVHD) and sepsis due to the breakdown of the gastrointestinal mucosa in patients (5). Other than careful fluid replacement and

Received 9 April 2018 **Returned for modification** 2 May 2018 **Accepted** 8 August 2018

Accepted manuscript posted online 13 August 2018

Citation Dang W, Xu L, Ma B, Chen S, Yin Y, Chang K-O, Peppelenbosch MP, Pan Q. 2018. Nitazoxanide inhibits human norovirus replication and synergizes with ribavirin by activation of cellular antiviral response. Antimicrob Agents Chemother 62:e00707-18. https://doi.org/10.1128/AAC.00707-18.

Copyright © 2018 American Society for Microbiology. All Rights Reserved.

Address correspondence to Qiuwei Pan, q.pan@erasmusmc.nl.

L.X. and B.M. contributed equally to this work.

intensive supportive care, no specific antivirals are currently available for treating norovirus gastroenteritis.

Nitazoxanide (NTZ) was developed in the early 1970s and originally commercialized as an antiparasitic drug. Following oral administration, NTZ is absorbed from the gastrointestinal (GI) tract and rapidly hydrolyzed by plasma esterase to form its active circulating metabolite, tizoxanide (TIZ). The concentration of TIZ in serum reaches a maximum of 10 μg/ml (6). Both drugs belong to a class of agents known as thiazolides (TZD). Currently, NTZ is licensed in the United States (Alinia; Romark Laboratories) for treating diarrhea caused by *Cryptosporidium parvum* and *Giardia intestinalis* in adults and children above 12 months of age (7). Interestingly, NTZ has also been reported to exert potent and broad-spectrum antiviral activity against many viruses, including influenza virus, hepatitis B virus (HBV), hepatitis C virus (HCV), human immunodeficiency virus (HIV), and rotavirus (7, 8). Mechanistically, it has been demonstrated that NTZ selectively blocks the maturation of the viral hemagglutinin of influenza viruses at the posttranslational level, thus inhibiting the proper assembly and release of the virus from host cells (9). With regard to HCV, NTZ is involved in activation of PKR, a key kinase that regulates the host innate anti-HCV response (10). For rotavirus, NTZ reduces the size and alters the architecture of rotavirus viroplasm, thus decreasing viral double-stranded RNA (dsRNA) formation (8). Recently, NTZ has been reported to elicit antiviral innate immunity to combat HIV and other virus infections (11). However, a general consensus regarding the antiviral mechanism of action of NTZ is not well established, and it seemingly depends on the virus itself and host cells.

Several clinical studies have recently demonstrated the off-label use of NTZ in treating norovirus gastroenteritis. In a randomized double-blind placebo-controlled clinical trial, 50 adults and adolescents presenting diarrhea with stools positive for norovirus, rotavirus, or adenovirus were enrolled. The median resolution time for all the subjects, including those infected with norovirus, was significantly reduced in the NTZ-treated group compared with the placebo group (12). Later, in a retrospective study comprising 12 patients with norovirus gastroenteritis after chemotherapy and hematopoietic stem cell transplantation (HSCT), 11 patients clinically responded with improvement in symptoms following NTZ administration (5). Similar results were observed in another study comprising 5 patients with norovirus gastroenteritis after HSCT. Oral administration of NTZ resulted in resolution of gastroenteritis and complete viral clearance (13). These clinical studies indicate the potential for repurposing NTZ as a viable therapeutic option for norovirus gastroenteritis. However, further experimental research is required to characterize its *bone fide* antinorovirus activity and to provide mechanistic insight. In a review article based on personal communication, it was mentioned that the 50% inhibitory concentration (IC_{50}) and IC_{90} for TIZ were 0.5 and 1.2 μg/ml, respectively, using a human norovirus (HuNV) replicon (7). In our previous study, we also found that NTZ displayed potent antinorovirus activity using the same replicon model (14). However, the exact antiviral mechanisms of NTZ against norovirus have not been revealed. Therefore, we have systematically explored the antinorovirus potential of TZD and studied its potential mechanism of action. Our results have revealed that TZD triggers a cellular innate immune response to combat norovirus replication and that it synergizes with ribavirin, a broad-spectrum antiviral drug that shows effectiveness against norovirus gastroenteritis *in vivo* (15).

RESULTS

TZD exhibited potent antiviral activity toward HuNV and FeCV replication without significant cytotoxicity. A Huh7 cell-based HuNV replicon model (HG23 cells), representing one of very few options in modeling HuNV replication in cell culture, has been widely used for studying antinorovirus agents. After 2 days of treatment, NTZ and TIZ dose-dependently inhibited HuNV replication (Fig. 1A). The toxicity of TZD toward HG23 cells was determined by MTT [3-(4,5-dimethyl-2-thiazolyl)-2,5-diphenyl-2H-tetrazolium bromide] assay. TZD showed no major toxicity toward HG23 cells at the

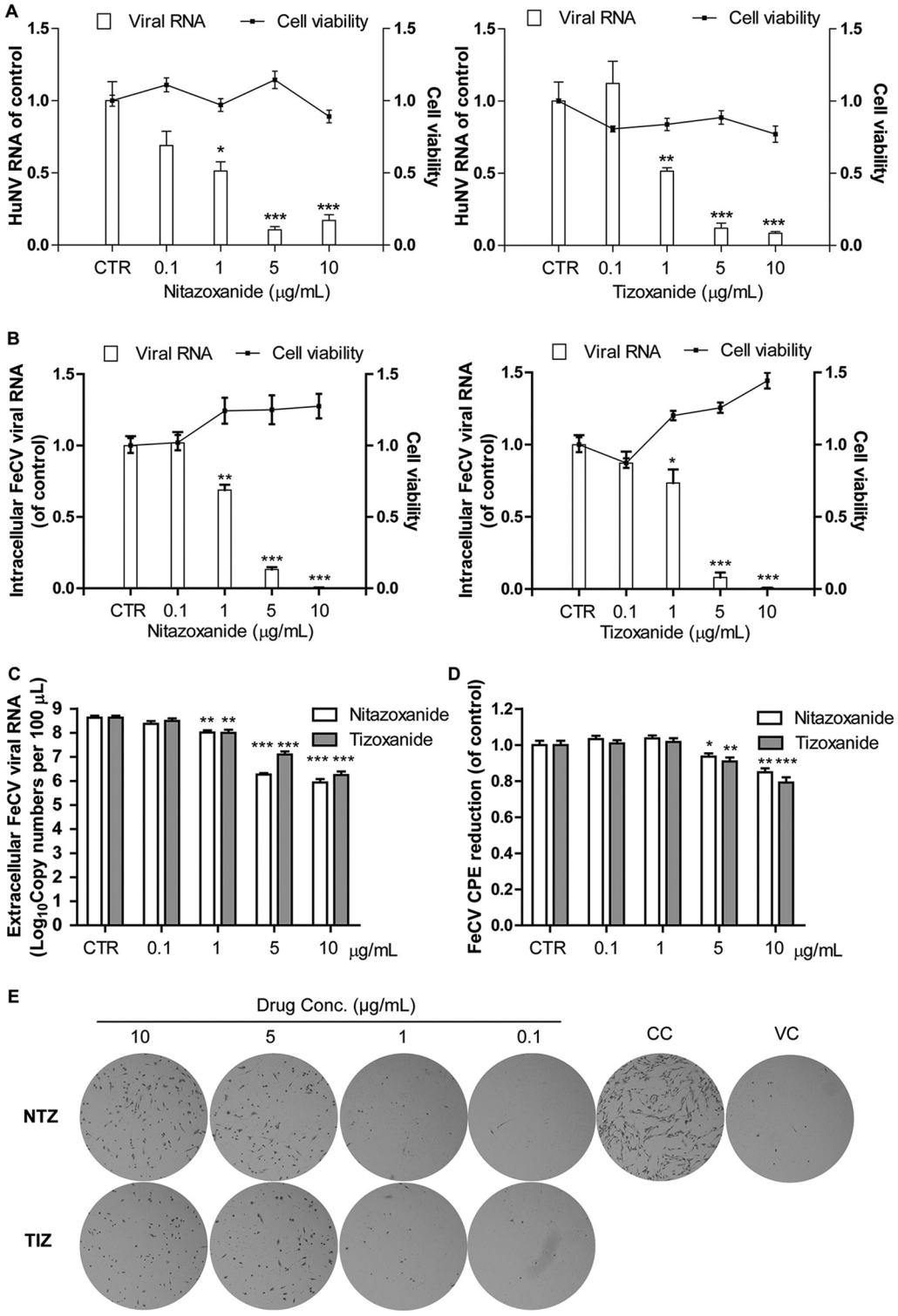

FIG 1 TZD potently inhibited replication of HuNV and its surrogate FeCV without significant cytotoxicity. (A) Nitazoxanide and its active metabolite tizoxanide dose-dependently inhibited HuNV replication without clear toxicity to host cells after 2 days of treatment. The level of HuNV replicon RNA was quantified using qRT-PCR and compared to that of vehicle control (0.05% DMSO, set as 1) (CTR) ($n = 3$ independent experiments, each in duplicate). (B) TZD elicited potent antiviral potential against FeCV. CRFK cells were first infected with FeCV (at an MOI of 0.1) and incubated with vehicle control or increasing concentrations of TZD. After 24 h of treatment, the cellular FeCV RNA level was quantified by qRT-PCR, normalized to that of feline GAPDH, and compared to vehicle control (set as 1). (C) Same as panel B for detecting cellular FeCV RNA; viral RNA copy numbers in the supernatant (secreted viruses) were also detected after 24 h of treatment with vehicle control or TZD. TZD significantly reduced extracellular FeCV RNA in the supernatant ($n = 3$ independent experiments, each in duplicate). (D and E) The anti-FeCV activity of TZD was further validated by an MTT- and hematoxylin and eosin staining-based CPE

(Continued on next page)

clinically relevant concentration of 10 μg/ml (Fig. 1A). These results demonstrate the potent antinorovirus effect of TZD without triggering major cytotoxicity.

Consistently, TZD dose-dependently reduced cellular viral RNA and virus production by a norovirus surrogate, feline calicivirus (FeCV), in the supernatant after 24 h of treatment without significant cytotoxicity (Fig. 1B and C). The inhibitory effect was also confirmed in a cytopathic effect (CPE) reduction assay, demonstrating that TZD at 5 and 10 μg/ml protected Crandell Rees feline kidney (CRFK) cells from FeCV-induced CPE formation (Fig. 1D). Meanwhile, TZD at 5 and 10 μg/ml significantly increased the survival of FeCV-infected CRFK cells (Fig. 1E). Collectively, our results demonstrated that TZD potently inhibited replication of HuNV and its surrogate, FeCV.

TZD activated the expression of ISGs, especially IRF-1. TZD has been recently reported to stimulate innate antiviral immunity in peripheral blood mononuclear cells *in vitro*, potentially accounting for its anti-HIV activity (11). Interferon (IFN) signaling is a vital component of the innate immunity against viral pathogens. It signals through the Janus kinase-signal transducers and activators of transcription (JAK-STAT) pathway and transcriptionally induces hundreds of interferon-stimulated genes (ISGs) as ultimate antiviral effectors (16, 17). We therefore investigated the antiviral state in HG23 cells after TZD treatment. Treatment with 10 μg/ml NTZ or TIZ for 2 days induced the expression of a panel of important ISGs, including interferon regulatory factor 1 (IRF-1), IRF-9, RIG-I, IFI27, PKR, ISG15, Mx1, and MDA5 (Fig. 2A). Some of these ISGs exerted broad activities against many viruses (18). Interestingly, compared with exogenous alpha interferon (IFN-α) (1,000 IU/ml), serving as a positive control, TZD were more potent at inducing IRF-1 mRNA expression (NTZ [fold change, 11.26 $\pm$ 1.94] versus TIZ [8.26 $\pm$ 1.70] versus IFN-α [4.89 $\pm$ 0.75]) (Fig. 2A). Western blot analysis confirmed the potent induction of IRF-1 in response to TZD treatment at the protein level (Fig. 2B; see the supplemental material). We next excluded the implication of HuNV replicon in TZD stimulation of ISGs, as TZD treatment also induced ISGs in naive Huh7 cells. Consistent with HG23 cell results, IRF-1 mRNA was stimulated by TZD more effectively than by 1,000 IU/ml IFN-α in Huh7 cells (NTZ [17.31 $\pm$ 2.94] versus TIZ [14.86 $\pm$ 3.49] versus IFN [2.57 $\pm$ 0.17]) (Fig. 2C).

TZD robustly induced ISGs in a human intestinal cell line and primary organoids. Though the cellular tropism of HuNV is not completely understood, the GI tract is believed to be the reservoir of HuNV replication. We further extended TZD treatment to human intestinal epithelial (Caco-2) cells and primary human intestinal organoids that recapitulated the nature of the intestinal epithelium (Fig. 2D). Consistently, TZD triggered an antiviral response in the two models, though to a lesser extent than with HG23 cells and Huh7 cells (Fig. 2E and F). TZD stimulated higher or comparable levels of IRF-1 mRNA than 1,000 IU/ml IFN-α in the two models.

Although the expression levels and patterns of ISGs differed among different cell models after TZD treatment, IRF-1 was consistently highly induced. IRF-1 has been reported to be one of the most important ISGs, exerting antiviral activities against 14 different viruses within 7 families (19). Therefore, we further specifically investigated the role of IRF-1 in TZD-mediated inhibition of HuNV replication.

IRF-1 inhibited HuNV replication and contributed to the TZD-mediated antinorovirus effect. To dissect the role of IRF-1 in HuNV replication, we first overexpressed IRF-1 in HG23 cells. A bicistronic lentiviral vector coexpressing IRF-1 and the red fluorescent protein TagRFP, as well as a control virus containing a luciferase (Fluc) gene from *Photinus pyralis* were used in the study (18). IRF-1 mRNA and protein levels were significantly increased in overexpressing cells after 2 days of transduction (Fig. 3A).

FIG 1 Legend (Continued)
reduction assay. CRFK cells were first infected with FeCV (at an MOI of 0.5) and incubated with vehicle control or TZD. After 2 days of treatment, the CPE was quantified by MTT assay, and residual cells were observed after fixation and staining with hematoxylin and eosin. In panel E, CC and VC represent cell control and virus control, respectively. The images are representative of three independent experiments. The data are presented as means $\pm$ SEM (*, $P < 0.05$; **, $P < 0.01$; ***, $P < 0.001$).

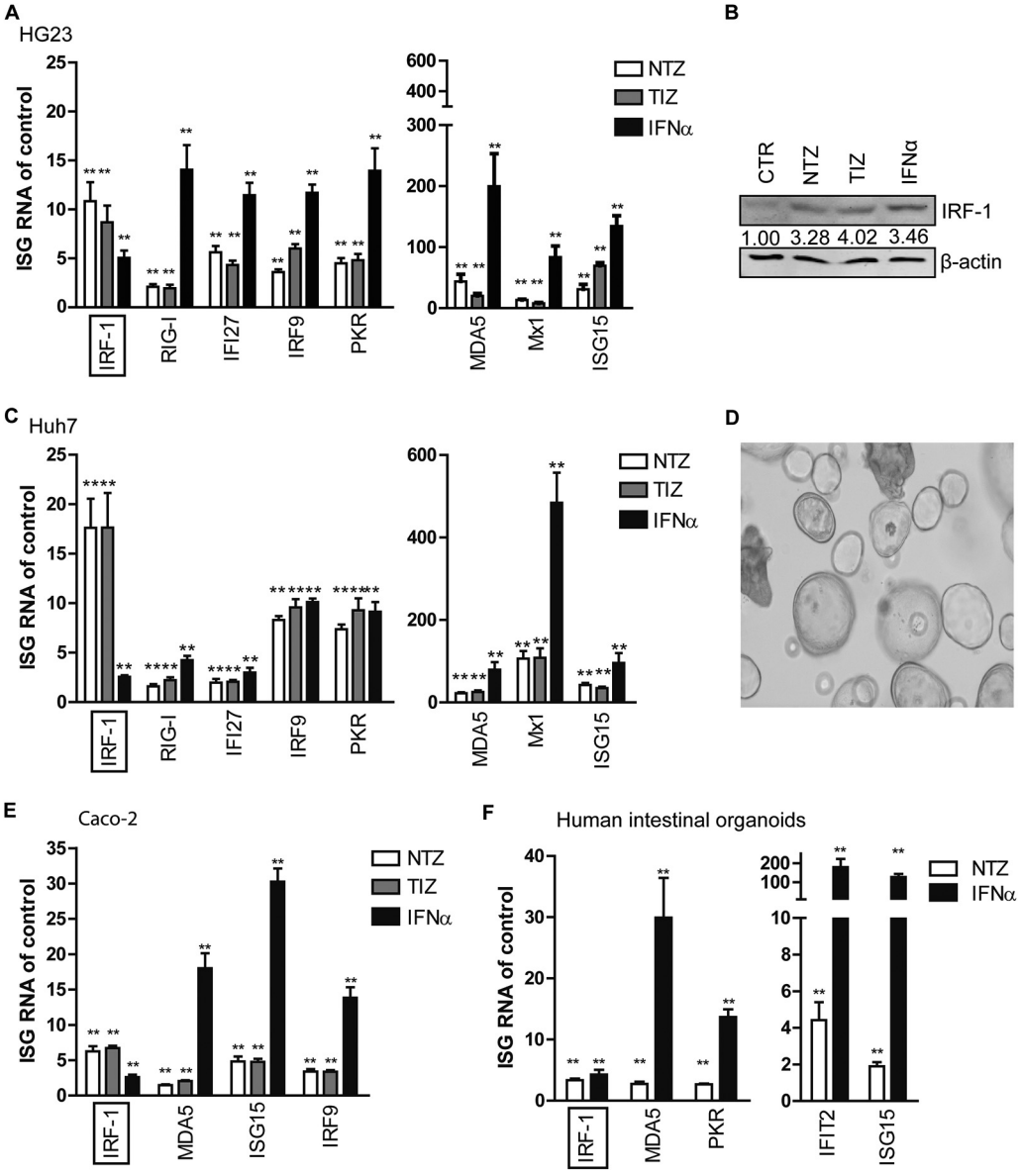

FIG 2 TZD robustly stimulated the expression of IRF-1 and several other ISGs in a HuNV replicon model and intestinal models of Caco-2 cells and primary organoids. (A) Fold changes of ISGs induced by NTZ (10 μg/ml), TIZ (10 μg/ml), or IFN-α (1,000 IU/ml) in HG23 cells. After 2 days of treatment, the levels of ISG mRNA were quantified by qRT-PCR and normalized to those of human GAPDH. The results are expressed as fold changes compared to the vehicle control (DMSO; $n = 3$ independent experiments, each in duplicate). (B) Western blot analysis of IRF-1 protein expression in response to NTZ (10 μg/ml), TIZ (10 μg/ml), or IFN-α (1,000 IU/ml). The data are representative of the results of three independent experiments. (C) Naive Huh7 cells were treated with NTZ (10 μg/ml), TIZ (10 μg/ml), IFN-α (1,000 IU/ml), or vehicle control. After 2 days of treatment, relative levels of ISG mRNA were quantified by qRT-PCR ($n = 3$ independent experiments, each in duplicate). (D) Morphology of 3D human primary intestinal organoids in Matrigel. (E) Relative levels of ISG RNA were quantified by qRT-PCR after 2 days of treatment with NTZ (10 μg/ml) or IFN-α (1,000 IU/ml) in Caco-2 cells ($n = 3$ independent experiments, each in duplicate). (C) Relative levels of ISG RNA in human intestinal organoids after treatment with NTZ (10 μg/ml) or IFN-α (1,000 IU/ml) for 2 days ($n = 3$ independent experiments, each in duplicate). The data are presented as means and SEM (*, $P < 0.05$; **, $P < 0.01$).

Exogenous IRF-1 overexpression resulted in robust inhibition of HuNV RNA replication, by 94.4% $\pm$ 2.9% (Fig. 3B). To further explore the role of basal IRF-1, a loss-of-function assay was performed to silence IRF-1 by transducing a lentivirus-based short hairpin RNA (shRNA) construct targeting IRF-1. A nontargeting scrambled vector was used as a control. Successful knockdown of endogenous IRF-1 was confirmed by quantitative real-time PCR (qRT-PCR) (by 52.4% $\pm$ 9.1%) and Western blot analysis (by 72%) (Fig. 3C).

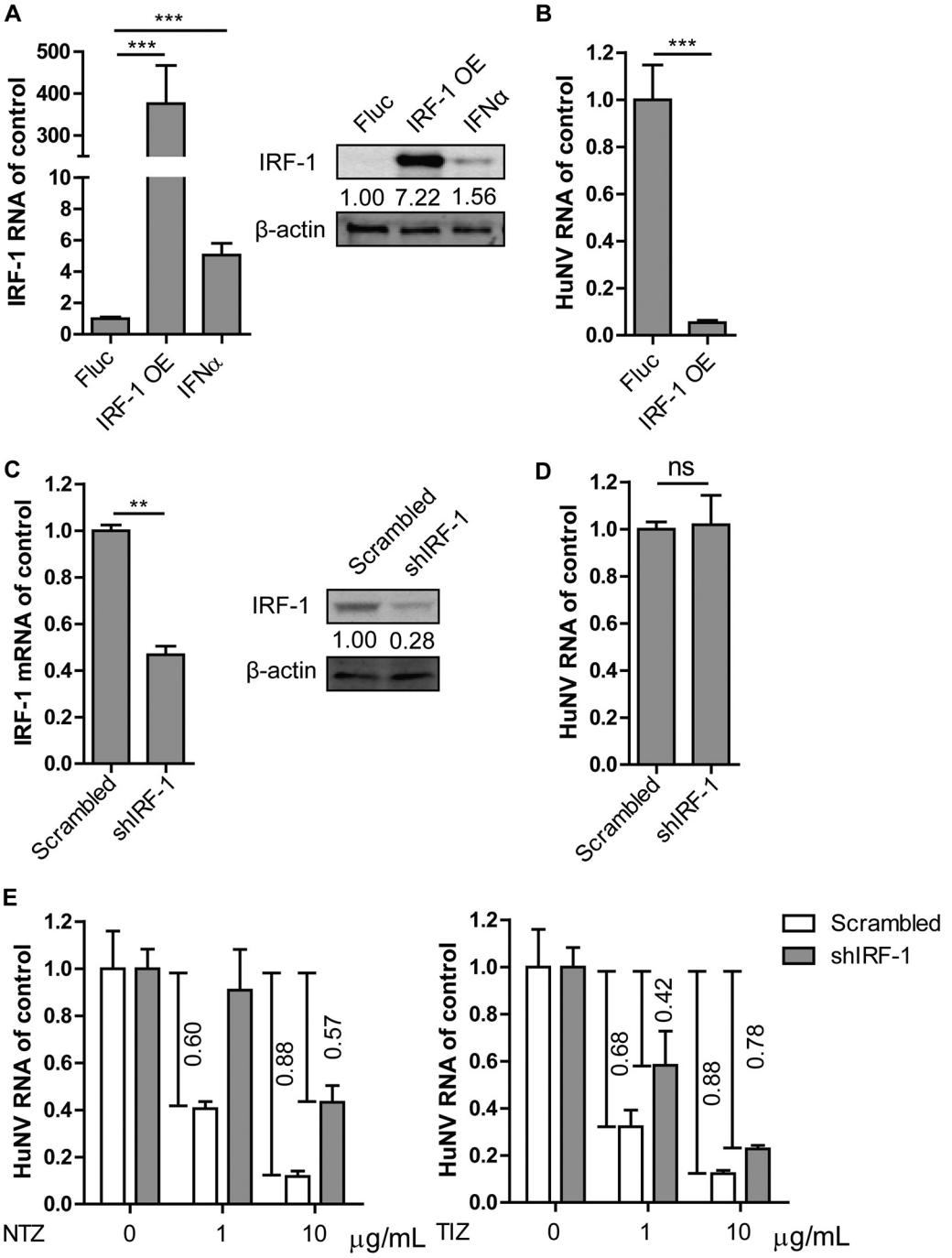

FIG 3 IRF-1 mediated TZD-triggered inhibition of HuNV replication. (A) To overexpress (OE) IRF-1, HG23 cells were transduced with lentiviral IRF-1-expressing vector or Fluc-expressing vector (control). After 2 days of transduction, the levels of IRF-1 expression were detected by qRT-PCR ($n = 3$ independent experiments, each in duplicate) and Western blotting ($n = 3$ independent experiments). IFN-α (1,000 IU/ml) was used as a positive control. (B) Overexpression of IRF-1 potently inhibited HuNV replication ($n = 3$ independent experiments, each in duplicate). (C) To further evaluate the role of basal IRF-1 in HuNV replication, HG23 cells were transduced with lentiviral shRNA vector targeting IRF-1. A scrambled vector was used as a nontargeting control. Successful knockdown of IRF-1 was confirmed by qRT-PCR ($n = 3$ independent experiments, each in duplicate) and Western blotting ($n = 3$ independent experiments). (D) Knockdown of IRF-1 had minor effects on HuNV replication ($n = 3$ independent experiments, each in duplicate). (E) IRF-1 shRNA and nontargeting control cells were mock treated or treated with the indicated concentrations of TZD. After 2 days of treatment, the levels of HuNV RNA were quantified by qRT-PCR and compared to those of the respective control ($n = 3$ independent experiments, each in duplicate). The data are presented as means and SEM (**, $P < 0.01$; ***, $P < 0.001$; ns, not significant).

In the absence of TZD, IRF-1 knockdown had a minor effect on HuNV RNA replication (Fig. 3D). However, the antinorovirus effects of TZD were largely attenuated in IRF-1 knockdown cells compared with control cells. This attenuated effect of TZD treatment was greater than that of TIZ (Fig. 3E). These results indicate that IRF-1 exerts antiviral activity and contributes to TZD-mediated inhibition of HuNV replication.

TZD triggering of the antiviral response was independent of the JAK-STAT pathway. To elucidate the mechanism by which TZD stimulated cellular antiviral immunity, we first examined whether TZD induced the production and secretion of IFNs. IFN genes, including IFN-α and IFN-β genes, and interleukin 28A/B (IL-28A/B) genes were detected in HG23 cells and intestinal organoids following NTZ treatment. NTZ unexpectedly showed minor effects on IFN mRNA expression (see the supplemental material).

The JAK-STAT pathway is the principal cascade for IFN signaling. Upon binding to the two IFN receptor subunits (IFNAR1 and IFNAR2), type I IFNs activate the Janus kinases (Jak1 and Tyk2) and signal transducers of transcription (STAT1 and STAT2), resulting in elevation of the levels of hundreds of ISGs. To examine whether TZD stimulated ISGs through the JAK-STAT pathway, TZD were combined with CP-690550 (tofacitinib), a potent and selective JAK inhibitor. IFN-α (100 IU/ml) was used as a control. The antiviral activity of IFN-α was partially abolished and HuNV RNA levels were restored from 4.5% $\pm$ 1.7% to 28.9% $\pm$ 14.6% when TZD were combined with CP-690550 (Fig. 4A). In contrast, CP-690550 did not interfere with the antinorovirus effect of TZD. Correspondingly, CP-690550 significantly suppressed IFN-α- but not TZD-mediated induction of ISGs, including IRF-1 (Fig. 4B), PKR, ISG15, and MDA5 (Fig. 4C).

STAT1 is a key component of the JAK-STAT pathway. A CRISPR/Cas9-mediated approach was used to efficiently knock out STAT1 in Huh7 cells. Successful knockout (KO) was confirmed by Western blotting. Compared with Huh7 control cells, STAT1 protein was undetectable in Huh7 KO cells (Fig. 4D). To further confirm the complete knockout of STAT1, Huh7 control and KO cells were treated with IFN-α. As expected, IFN-α treatment (1,000 IU/ml) significantly induced STAT1 expression in Huh7 control cells, but not in KO cells, while no major difference was observed in STAT2 mRNA in both types of cells (Fig. 4E). These data indicated the successful knockout of STAT1. Next, Huh7 control and KO cells were treated with TZD or 1,000 IU/ml IFN-α for 2 days, and the expression of ISGs was measured by qRT-PCR. We first observed that STAT1 KO slightly decreased the basal levels of a subset of ISGs, including MDA5, Mx1, and DDX60. This was probably due to the fact that STAT1 is critical to maintain cellular innate immune homeostasis. As expected, the induction levels of ISGs in KO cells were significantly diminished in response to IFN-α treatment compared with control cells. However, TZD induced similar levels of ISGs in both control cells and KO cells, including IRF-1 (Fig. 4F), MDA5, Mx1, DDX60, ISG15, and IFIT1 (Fig. 4G), suggesting that TZD induced an antiviral response and ISG expression independently of the JAK-STAT pathway.

Nuclear factor-kappa B (NF-κB) signaling participates in modulating the activation of various proinflammatory cytokine genes and ISGs (20), contributing to a vital role in combating pathogen invasion. By using Huh7 and Caco-2 cell-based NF-κB luciferase reporter cells, we further excluded the activation of the NF-κB pathway by TZD (see the supplemental material). Thus, a novel mechanism is likely involved in the TZD-induced cellular antiviral response.

Synergistic antinorovirus activity and augmented ISG induction by TZD and ribavirin combination. To achieve better antiviral efficacy, we evaluated the effect of a combination of TZD and ribavirin against HuNV replication. In short-term (2-day) treatment, a combination of NTZ and ribavirin did not achieve significantly enhanced inhibition of HuNV replication and showed an additive effect as calculated with Mac Synergy II software (Fig. 5A). Similar results were observed for a TIZ and ribavirin combination (Fig. 5B).

We next prolonged the treatment time in a long-term (10-day) assay, and HuNV RNA was quantified after 2, 6, and 10 days of treatment. Importantly, NTZ in combination

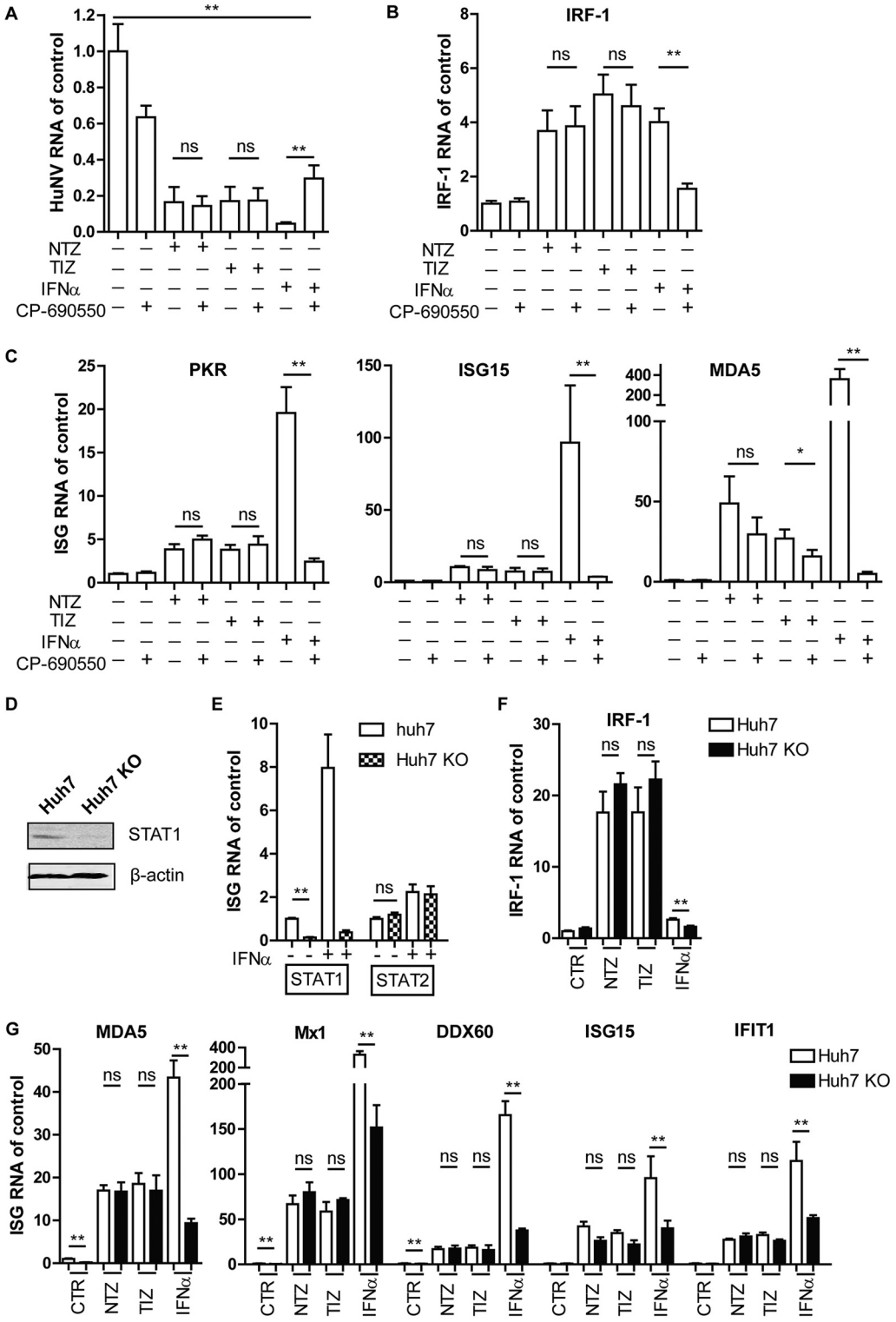

FIG 4 Stimulation of antiviral response by TZD was independent of the JAK-STAT pathway. (A) HG23 cells were treated with vehicle only (DMSO; control), NTZ (10 μg/ml), TIZ (10 μg/ml), or IFN-α (100 IU/ml) alone or in combination with CP-690550 (1,000 ng/ml). After 2 days of treatment, HuNV replication was quantified by qRT-PCR (n = 3 independent experiments, each in duplicate). (B and C) The expression of IRF-1 and other ISGs, including PKR, ISG15, and MDA5, was quantified by qRT-PCR (n = 3 independent experiments, each in duplicate). (D) A STAT1 KO clone was established from Huh7 cells expressing STAT1 sgRNAs. Successful KO of STAT1 was confirmed by Western blotting. (E) To further confirm successful KO of STAT1, Huh7 control and STAT1 KO cells were treated with IFN-α (1,000 IU/ml) for 2 days. The levels of STAT1 and STAT2 RNA were evaluated by qRT-PCR (n = 3 independent experiments, each in duplicate). KO of STAT1 abolished the induction of STAT1, but not STAT2, after IFN-α treatment. (F and G) Huh7 control and STAT1 KO cells were mock treated (DMSO;

(Continued on next page)

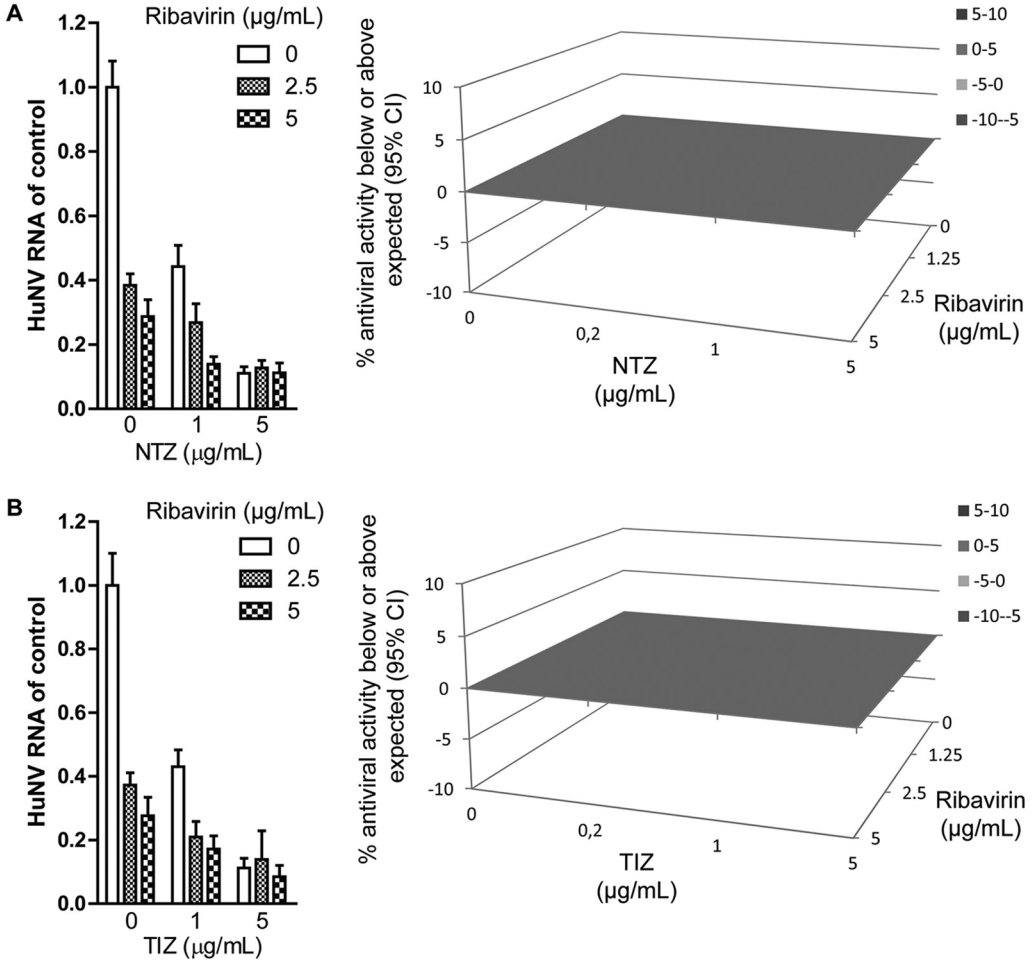

FIG 5 TZD worked additively with ribavirin to inhibit HuNV replication after short-term treatment. (A) HG23 cells were treated with various concentrations of NTZ alone, ribavirin alone, or the two in combination for 2 days. (Left) Antiviral activities were determined by qRT-PCR ($n = 3$ independent experiments, each in duplicate). (Right) To further explore the drug-drug interaction, the antiviral results were analyzed with a mathematical model. The 3D surface plot shown represents the difference (within a 95% confidence interval [CI]) between actual experimental effects and the theoretical additive effect of the combination at various concentrations of the two compounds. (B) Combination of TIZ with ribavirin. The error bars represent SEM.

with ribavirin resulted in enhanced inhibition of HuNV replication after prolonged treatment (Fig. 6A). Antiviral data at 10 days suggested a potent synergistic effect in combination, as shown in the three-dimensional (3D) Mac Synergy II plot (Fig. 6B). To further detect the residual HuNV replicons in host cells after prolonged combination treatment, a rebound assay was designed by culturing HG23 cells with the selection marker G418. If HuNV replicons were completely deleted from host cells, HG23 cells could not proliferate to form colonies. As shown In Fig. 6C, no colonies were found with the combination of 2.5 μg/ml NTZ and 5 μg/ml ribavirin, indicating the complete clearance of HuNV replicons from host cells. To gain more evidence to support this finding, a gel-based RT-PCR assay was performed to specifically detect HuNV replicons in the cell culture RNA. No bands were detectable after high-concentration combination treatment, confirming the depletion of HuNV replicons from host cells (see the

FIG 4 Legend (Continued)
control) or treated with NTZ (10 μg/ml), TIZ (10 μg/ml), or IFN-α (1,000 IU/ml). After 2 days of treatment, the expression levels of IRF-1, MDA5, Mx1, DDX60, ISG15, and IFIT1 were detected by qRT-PCR. The results were first normalized to human GAPDH and then compared to control cells ($n = 3$ independent experiments, each in duplicate). The data are presented as means and SEM (*, $P < 0.05$; **, $P < 0.01$; ns, not significant).

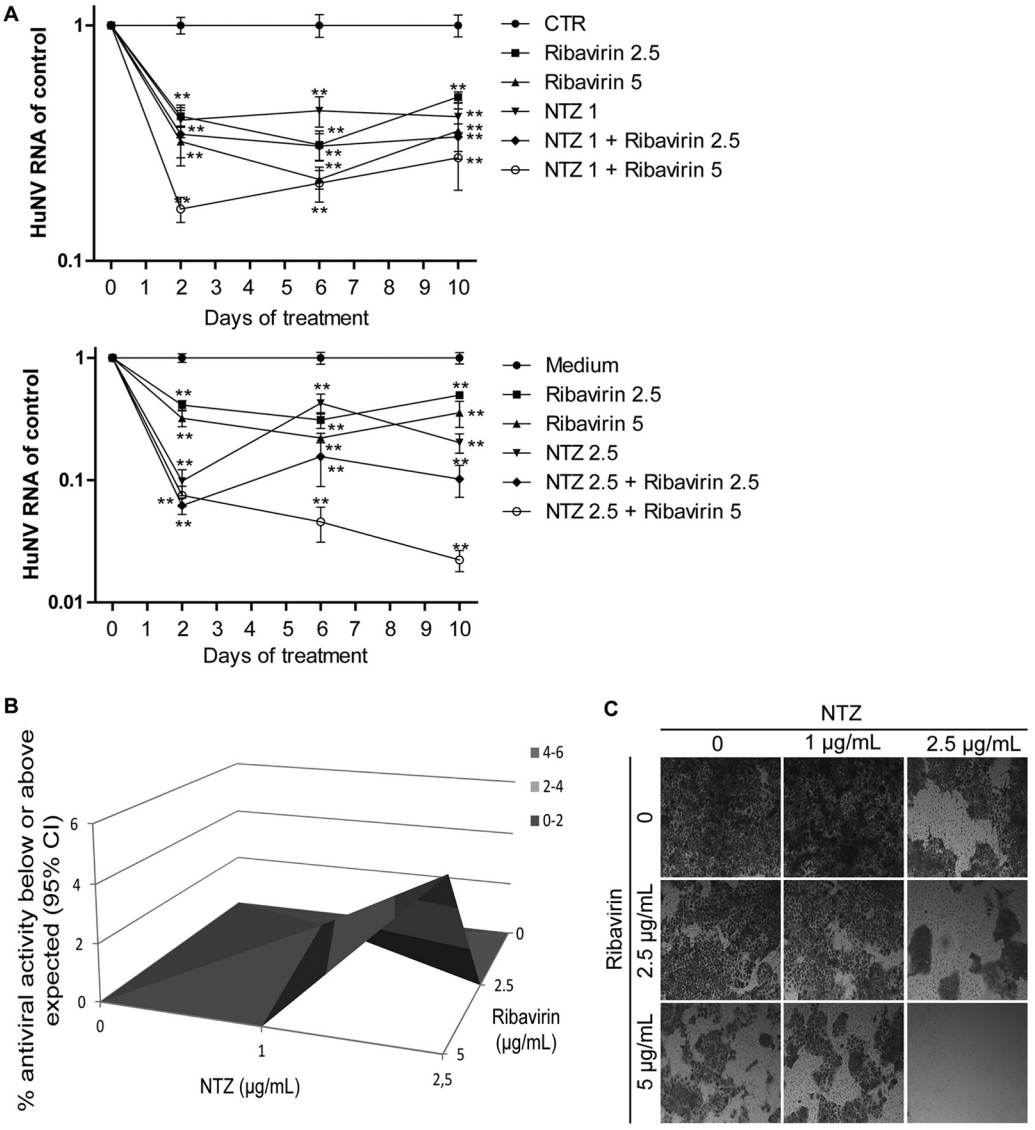

FIG 6 Long-term combination of NTZ with ribavirin synergistically inhibited HuNV replication and completely depleted HuNV replicons from host cells. (A) HG23 cells were incubated with NTZ alone, ribavirin alone, or the two drugs in combination. After 2 days of culture, the cells were passaged to fresh drug-containing medium for another 4 days of incubation. After 6 days, the cells were passaged with another round of 4 days of treatment. At the end of each treatment, the HG23 cells were harvested and analyzed for levels of HuNV RNA ($n = 3$ independent experiments, each in duplicate). (B) Synergy analysis. The antiviral results after 10 days of treatment were analyzed with MacSynergy. (C) Rebound assay. After 10 days of treatment, HG23 cells were plated into a 48-well plate (2×10^5 cells per well) containing 250 μl medium with 1 mg/ml G418. After 5 days of culture, the cell colonies were stained and visualized using an inverted light microscope. The data presented are representative of 3 independent experiments. The data are presented as means ± SEM (**, $P < 0.01$).

supplemental material). Similar results were obtained with the TIZ and ribavirin combination (Fig. 7; see the supplemental material). Concurrently, we observed synergistic induction of ISGs in combination treatment, including IRF-1, MDA5, PKR, and Mx1 (Fig. 8). Of note, this synergistic induction of ISGs was modest on day 2 but more robust on days 6 and 10 (Fig. 8). This may support the combined antinorovirus effects of TZD and ribavirin, which were additive in short-term treatment but synergistic after long-term treatment.

DISCUSSION

Norovirus has become the most common cause of virus-induced diarrheal cases for all ages following introduction of rotavirus vaccine (21). In healthy general populations,

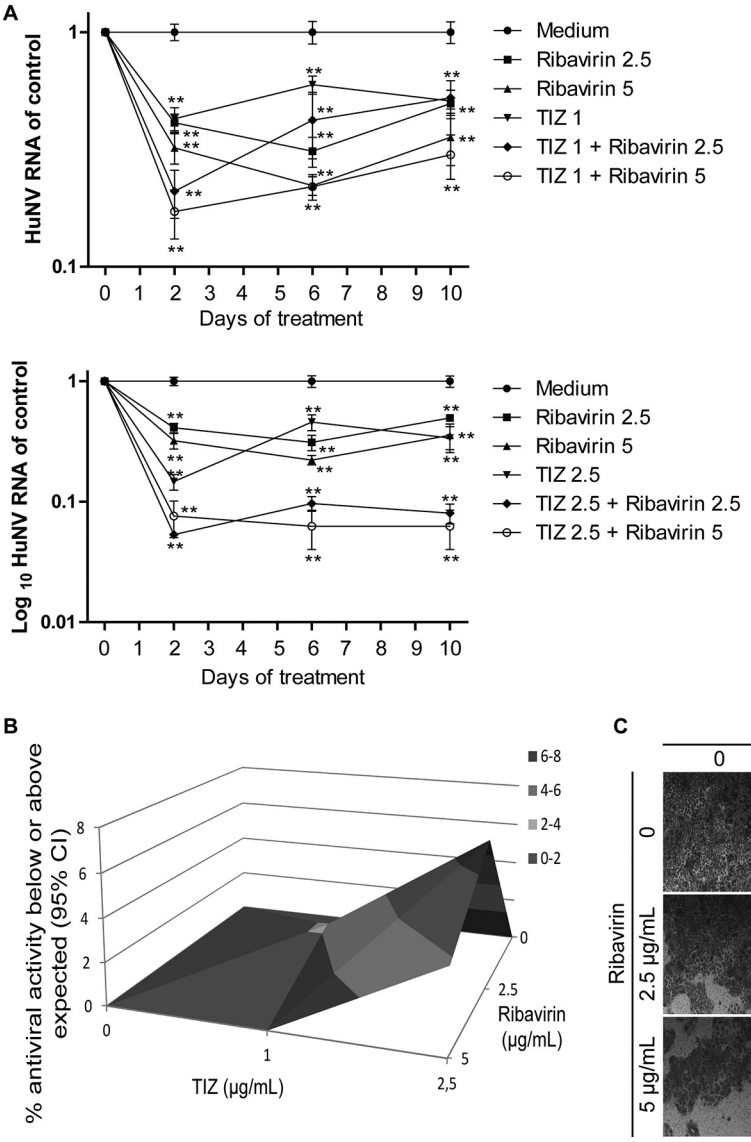

FIG 7 Combining TIZ with ribavirin synergistically inhibited HuNV replication. (A) Combination of TIZ with ribavirin showed greater efficacy against HuNV replication than the individual drugs ($n = 3$ independent experiments, each in duplicate). (B) Synergy analysis. (C) Rebound assay after long-term treatment. The data are presented as means ± SEM (**, $P < 0.01$).

norovirus normally causes self-limiting gastroenteritis. However, it often results in prolonged symptoms and virus shedding in immunocompromised patients. In a retrospective study comprising 2,183 solid-organ transplant (SOT) recipients, 4.6% of the recipients were diagnosed as norovirus positive, and 22.8% of them developed chronic norovirus gastroenteritis (22). Meanwhile, norovirus gastroenteritis is a great global economic burden due to the resulting huge health system costs and productivity losses (1). Some clinical studies have reported the successful use of human immunoglobulin (HIG) (23) and ribavirin (24) for empirical treatment. Due to inadequate clinical data and experimental studies, both drugs require further evaluation as potential therapies. NTZ was recently demonstrated to be effective therapy for norovirus gastroenteritis in immunocompromised patients (7). It showed high tolerance and minor adverse effects even after several weeks of administration in those patients (5). Here, we documented that TZD exerted potent antinorovirus efficacy by inducing an innate antiviral response, in particular IRF-1, in a HuNV replicon (HG23 cells). It exhibited synergistic antinorovirus activity with ribavirin, which supports the potential of the combination treatment.

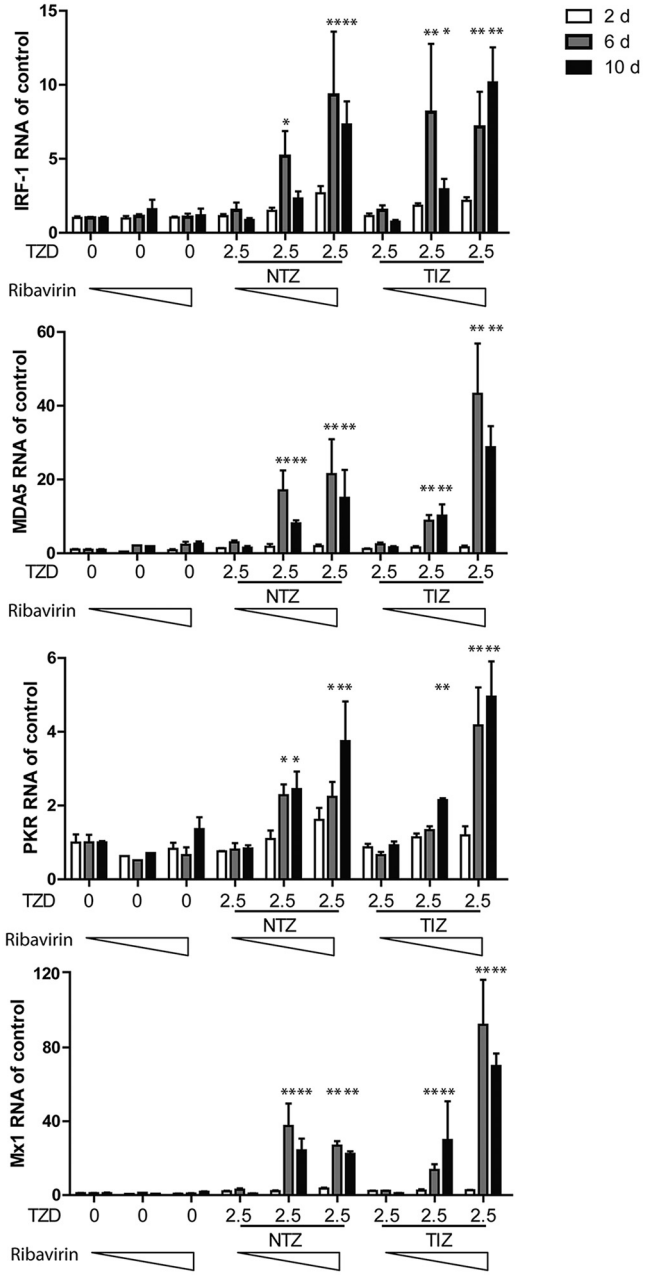

FIG 8 Augmented induction of ISGs after combination treatment with TZD and ribavirin. Shown are qRT-PCR analysis of expression levels for IRF-1, MDA5, and PKR after treatment with TZD (NTZ, 2.5 μg/ml; TIZ, 2.5 μg/ml) and ribavirin (0, 2.5, and 5 μg/ml) in HG23 cells for 2, 6, and 10 days (d) ($n = 3$ independent experiments, each in duplicate). The error bars indicate SEM.

The HuNV replicon represents one of the few options for anti-HuNV drug evaluation. However, it does not fully recapitulate the HuNV life cycle, with deficiency of viral attachment, entry, assembly, and release. Meanwhile, the relatively low replication level (ranging from 1,000 to 3,000 copies per cell) (25) may not fully resemble the peak amount of virus shedding, which reached 95×10^9 genomic copies/g feces in patients upon HuNV infection (26). The shortage of HuNV infection models prompted us to exploit HuNV surrogates to further confirm the antinorovirus properties of TZD. Murine norovirus (MNV) is a good model system to study norovirus biology and pathogenesis, as well as antiviral therapies (27). Surprisingly, NTZ exerted opposing effects on human and murine norovirus replication. A high concentration of NTZ (10 μg/ml) increased

MNV strain MNV-1 replication and elicited no effects on the replication of another two strains, MNV^{CW3} and MNV^{CR6} (14). FeCV belongs to the family *Caliciviridae* and possesses many biochemical characteristics, a genomic organization, and a primary RNA sequence similar to those of norovirus. Therefore, FeCV has been used as a surrogate model to study norovirus, especially the aspects of antiviral development, inactivation methods, and effective intervention in transmission (28–30). Moreover, FeCV could be persistently cultivated in CRFK cells. We have demonstrated similar anticalicivirus effects elicited by TZD against FeCV. These results collectively suggest that TZD possesses potent antiviral potential against HuNV.

NTZ was originally developed as an antiprotozoal agent and was later reported to be a broad-spectrum antiviral drug for many viruses, including influenza virus, rotavirus, HBV, HCV, HIV, yellow fever virus, and Japanese encephalitis virus (7). It has been repurposed for the treatment of influenza in a phase 2b/3 clinical trial (7). However, the exact mechanism of action has remained largely elusive. NTZ was previously reported to stimulate antiviral innate immunity, which contributed to its anti-HIV activity (11). In our study, we have demonstrated that TZD inhibits HuNV replication by inducing a panel of ISGs. Among the induced ISGs with generic antiviral effects, some were previously noted to have antinorovirus activity: (i) ISG15 mitigates MNV-1 replication *in vitro* and *in vivo* by targeting an early step in the viral life cycle (31); (ii) MDA5, a cellular sensor, recognized MNV-1 and further triggered a host immune response to MNV-1 (32); (iii) PKR mediated type II IFN inhibition of MNV-1 translation (33).

Intriguingly, IRF-1, a broad antiviral ISG, was potently induced by TZD at comparable or higher levels than by 1,000 IU/ml IFN-α treatment. This was observed in multiple cell types, including HG23, naive Huh7, and Caco-2 cells, and in primary intestinal organoids. Importantly, we demonstrated that IRF-1 possesses a potent antinorovirus effect and mediates the antiviral effects of TZD. Interestingly, IRF-1 by itself was able to induce the expression of many ISGs, resulting in a higher magnitude of antiviral immunity by inducing IFN production (34, 35) or by directing activation of the JAK-STAT pathway (36). Classically, transcription of ISGs occurs via the JAK-STAT pathway. By pharmacological and genetic approaches, we found that the induction of ISGs by TZD was independent of this cascade. Further studies also excluded the activation of the NF-κB pathway and production of IFNs from the actions of TZD. One possible mechanism of action in the upregulation of ISGs by TZD may be the inhibition of a transcriptional repressor. Accumulating evidence suggests that many DNA-binding proteins act as transcriptional repressors for the induction of ISGs (37). NTZ is involved in multiple biological processes, including interfering with crucial metabolic and prodeath signaling (38). Thus, NTZ may inhibit those transcriptional repressors, resulting in the induction of ISG expression. Further research is called for to reveal the exact mechanism of action.

Although NTZ has been used empirically in several cases for treating norovirus gastroenteritis (39–41), its efficacy has remained controversial. NTZ was reported to be ineffective in a patient with X-linked agammaglobulinemia (42). Ribavirin, a broad-spectrum antiviral agent, has been reported to inhibit norovirus *in vitro* (43). Clinical studies have demonstrated that ribavirin treatment resulted in complete viral clearance in a subset of patients but failed in others (24). In this study, a combination of the two regimens resulted in synergistic antinorovirus effects and could completely clear the virus replicons from host cells, even below or at clinically achievable concentrations. One potential antiviral mechanism of ribavirin was modulating cellular immunity and inducing ISGs (44). Consistently, we observed augmented induction of ISGs by a combination of TZD and ribavirin.

In summary, we have demonstrated the *bone fide* antinorovirus effects of TZD through induction of a cellular antiviral response. They further synergized with ribavirin in antiviral activity and ISG induction. This knowledge has important implications for repurposing NTZ or using it in combination with ribavirin for treating norovirus gastroenteritis.

MATERIALS AND METHODS

Cell lines and virus propagation. Human Huh7 hepatocellular carcinoma cells expressing HuNV genotype 1 replicons (HG23 cells) (25) and human embryonic kidney 293T (HEK293T) cells were cultured in Dulbecco's modified Eagle's medium (DMEM) (Lonza Verviers, Belgium) supplemented with 10% (vol/vol) heat-inactivated fetal calf serum (FCS) (HyClone, Logan, UT, USA), 100 μg/ml streptomycin, and 100 IU/ml penicillin. Caco-2 cells (human Caucasian colon adenocarcinoma; European Collection of Authenticated Cell Cultures [ECACC]) were cultivated in DMEM supplemented with 20% (vol/vol) FCS, 100 μg/ml streptomycin, and 100 IU/ml penicillin. Crandell Rees feline kidney (CRFK) cells were maintained in minimum essential medium with Earle's salts without glutamine (EME), 1% L-glutamine, 0.05% (wt/vol) sodium bicarbonate, 0.02 M HEPES buffer, 0.2% nystatin solution, 10% (vol/vol) fetal bovine serum (FBS), 100 μg/ml streptomycin, and 100 IU/ml penicillin. A neomycin resistance gene was engineered into open reading frame 2 (ORF2), thereby conferring resistance to gentamicin (G418; Gibco) on HG23 cells (25). G418 was added to HG23 culture medium at 1.5 mg/ml for selection before experimentation.

FeCV (a kind gift from Erwin Duizer, National Institute for Public Health and the Environment, Netherlands) strain F9 was propagated in monolayers of CRFK cells as previously described (45). Briefly, FeCV was inoculated into CRFK monolayers at a multiplicity of infection (MOI) of 0.1. After 3 days of incubation, the FeCV cultures were collected by repeated freezing and thawing and clarified by centrifugation at 4,000 rpm for 10 min. The supernatant was filtered through a 0.45-μm filter (Waters Millipore), titrated by 50% tissue culture infectious dose ($TCID_{50}$), and stocked at −80°C for all subsequent experiments.

Reagents. NTZ (Sigma-Aldrich; CAS number 55981-09-4), TIZ (Cayman Chemical; CAS number 173903-47-4), and CP-690550 (Santa Cruz Biotechnology; CAS number 477600-75-2) were dissolved in dimethyl sulfoxide (DMSO) at 20 mg/ml, 5 mg/ml, and 1 mg/ml, respectively. Ribavirin (Sigma-Aldrich; CAS number 36791-04-5) was stocked in water at 10 mg/ml. Human IFN-α2a recombinant protein (IFN-α) (Thermo-Fisher Scientific; catalog number 111001) was stocked in phosphate-buffered saline (PBS) containing 0.1% bovine serum albumin (BSA) at 100,000 U/ml based on international units. Matched concentrations of DMSO (0.05%) were used as vehicle controls. To avoid repeated freeze-thaws, the compounds were aliquoted and stored at −80°C. During experimentation, the compounds were stepwise diluted to the desired concentration.

IRF-1 (D5E4; rabbit monoclonal antibody [MAb]; number 8478) antibody was obtained from Cell Signaling Technology, and β-actin (C-4; mouse MAb; sc-47778) was purchased from Santa Cruz Biotechnology (Santa Cruz, CA, USA). Secondary antibodies, IRDye 800CW-conjugated goat anti-rabbit and goat anti-mouse IgGs (1:10,000; Li-Cor Bioscience, Lincoln, NE, USA), were used as appropriate.

Culturing and passaging of human primary intestinal organoids. Culture of human primary intestinal organoids was performed as described previously (46). Intestinal biopsy specimens were dissected, cut longitudinally, and completely washed with cold PBS. After removing villus and fat, the small intestine was minced into small pieces (~1 mm^3) in a 10-cm culture dish using a scalpel and washed with complete chelating solution (CCS) (1.0 g/liter $Na_2HPO_4 \cdot 2H_2O$, 1.08 g/liter KH_2PO_4, 5.6 g/liter NaCl, 0.12 g/liter KCl, 15 g/liter sucrose, 10 g/liter D-sorbitol, and 80 μg/liter DL-dithiothreitol dissolved in MilliQ H_2O) 3 times by pipetting up and down 15 times, followed by further incubation with 8 mM EDTA on a shaking platform for 15 min at 4°C. The supernatant was discarded, and the biopsy specimens were gently rinsed with PBS to completely eliminate the EDTA. The minced intestine was thoroughly suspended in CCS solution by pipetting up and down 10 times with a 10-ml pipette to loosen the crypts, and 2 ml FCS was added. The supernatant contained crypts and was collected in a 50-ml tube, whereas the remaining biopsy specimens were further digested with EDTA 2 or 3 times, and the supernatants with crypts were pooled. The crypt suspension was first centrifuged at 300 × *g* for 5 min. The supernatant was gently removed, and the pellet was resuspended in 2 ml complete medium growth factor (CMGF) (advanced DMEM/F12 [Gibco, reference no. 12634-010, lot no. 1961596] supplemented with 1% [vol/vol] GlutaMAX supplement [Gibco, Grand Island, NY, USA], 10 mM HEPES, and 100 U/ml penicillin-streptomycin). A second round of centrifugation at 130 × *g* for 5 min was performed to harvest the crypts. The crypt pellet was finally suspended in ice-cold growth factor reduced phenol red-free Matrigel (Corning, Bedford, MA, USA) and dropped into the center of a prewarmed (37°C) 24-well plate at 100 to 500 crypts per well. The plate was incubated at 37°C for 15 min for Matrigel solidification. Finally, the crypts were cultured in culture medium (see the supplemental material) and passaged every 6 days.

After approximately 6 days, the organoids were passaged. Briefly, organoids were collected in a 15-ml Falcon tube and dissociated mechanically by pipetting up and down 15 to 20 times by passing through a Gilson pipette (5 ml; Sarstedt, reference no. 86.1253.001) with a 200-μl tip. The resulting suspension was centrifuged at 150 × *g* for 5 min at 4°C, and the pellet was cultured in fresh Matrigel with a 1:3 split ratio.

HuNV antiviral assay. Twenty-four hours before experimentation, HG23 cells were cultured in medium without G418. HG23 cells were seeded into 48-well plates (2.5 × 10^4 cells per well) and treated with compounds alone or in combination, and HuNV RNA levels were quantified after 2 days of treatment by qRT-PCR using a primer pair targeting the RNA-dependent RNA polymerase (RdRP) of HuNV. To further evaluate the long-term effects of the compounds on HuNV replication, long-term treatment and rebound assays were designed, as described previously (14, 43, 47). During long-term treatment, HG23 cells were treated with compounds for 2, 6, or 10 days. The cells were passaged to avoid overgrowth, and the drugs were replenished between passages. At the end of each treatment period, HuNV RNA levels were determined by qRT-PCR. After 10 days of treatment, the compounds were omitted. The HG23 cells were plated in a 48-well plate (2.5 × 10^4 cells per well) and cultured under the selective pressure of G418 (1 mg/ml). Following 5 days of culture, the cell colonies were stained with hematoxylin and eosin and

visualized with an inverted Zeiss Axiovert 200 microscope equipped with a Zeiss AxioCam MRm camera (Zeiss LLC, Thornwood, NY, USA).

FeCV $TCID_{50}$ and antiviral assay. The FeCV stock was quantified by $TCID_{50}$ assay. Briefly, 50 μl of 10-fold dilutions of FeCV were inoculated into 100 μl of CRFK cells in a 96-well plate at 1,000 cells per well. After 5 days of incubation at 37°C, each well was scored under a light scope for CPE. A $TCID_{50}$ was calculated from 6 replicates by the Reed-Muench method.

The antiviral activity of TZD against FeCV was detected by qRT-PCR and CPE reduction assay. The antiviral assay with FeCV was initiated by inoculating the virus into CRFK monolayers at an MOI of 0.1 (2.5×10^4 cells per well of a 48-well plate). Following 90 min of incubation at 37°C, the cells were washed with PBS 3 times to remove free virus, and increasing concentrations of TZD were added. After 24 h of treatment, extracellular RNA and intracellular RNA were extracted from the supernatant (virus particles; 100 μl) and cell monolayers, respectively. The relative intracellular FeCV RNA levels were normalized to feline GAPDH (glyceraldehyde-3-phosphate dehydrogenase) and calculated by the $2^{-\Delta\Delta CT}$ method. To further quantify the absolute numbers of virus genomes in the supernatant, the FeCV genome copy number was detected by qRT-PCR using the following primer pair: forward primer, 5′-GAACTACCCGCCAATCAACAT-3′ (corresponding to nucleotides [nt] 2420 to 2440), and reverse primer, 5′-CGGCTCTGATGGCTTGAAACTG-3′ (corresponding to nt 2507 to 2528). Briefly, a cDNA-containing target sequence in FeCV was amplified using a Q5 high-fidelity DNA polymerase kit (New England BioLabs Inc.) in a 25-μl reaction mixture containing 5 μl 5× Q5 reaction buffer, 0.5 μl 10 mM deoxynucleoside triphosphates (dNTPs), 1.25 μl 10 μM forward primer (5′-GAACTACCCGCCAATCAACA T-3′; corresponding to nt 2420 to 2440), 1.25 μl of 10 μM reverse primer (5′-CGGCTCTGATGGCTTGAA ACTG-3′; corresponding to nt 2507 to 2528), 5 μl of template cDNA, and 0.25 μl of Q5 high-fidelity DNA polymerase. Amplification was carried out with initial denaturation at 98°C (30 s); 35 cycles of 98°C (10 s), 66°C (30 s), and 72°C (30 s); and an additional extension step of 72°C for 2 min. The product was subjected to agarose gel electrophoresis, purified using a Charge Switch-Pro PCR cleanup kit (Invitrogen), and 10 times serially diluted. The dilutions were quantified by qRT-PCR to generate a standard curve, which was expressed by plotting the log copy numbers against the cycle threshold (C_T) values (see the supplemental material). The FeCV genome copy numbers in the medium were calculated by comparing the C_T with that of the standard curve.

FeCV could induce significant CPE in CRFK cells (48). The antiviral activity of TZD on FeCV was further confirmed by using an MTT-based CPE induction assay. Briefly, 10 μl of FeCV was inoculated into 80 μl of CRFK cells (1×10^4 cells per well of a 96-well plate) at an MOI of 0.5, followed by addition of 10 μl of increasing concentrations of TZD. After 2 days of incubation, a clear CPE was observed, characterized by complete destruction of the cell monolayers in the control well. Then, an MTT assay was performed, and the absorbance (optical density [OD]) at 490 nm was recorded. CPE reduction was calculated as follows: $[(OD_{treated})_{FeCV} - OD_{VC}]/(OD_{CC} - OD_{VC})$, where $(OD_{treated})_{FeCV}$ represents the OD of virus-infected cells treated with drugs, while OD_{CC} and OD_{VC} represent the ODs of the cell control and virus control, respectively. The protective effect of TZD on FeCV-infected CRFK cells could also be directly visualized by observing the survival of the cells. In brief, each well was stained with hematoxylin and eosin and visualized with an inverted light microscope.

Drug treatment of Caco-2 cells and organoids. Caco-2 cells were plated in a 48-well plate (2×10^4 cells per well) and incubated with 10 μg/ml TZD. After 2 days of treatment, the medium was discarded and the cell monolayers were washed 3 times with PBS. The cells were subsequently lysed for RNA extraction.

The organoid experiment was performed on monolayer cultures of organoids, as described previously (49). A 24-well plate was precovered with 50% collagen R and incubated at 37°C for 30 min. Organoids were harvested, transferred to a 24-well plate (100 to 200 organoids per well), and centrifuged at 1,500 rpm for 10 min. The drug was added, and the cultures were further incubated for 48 h. After treatment, the supernatant was aspirated, and the monolayers were washed with PBS 3 times and lysed for qRT-PCR.

Generation of IRF-1-expressing lentiviral pseudoparticles and lentiviral transduction. HEK293T cells were used to generate IRF-1-expressing lentivirus vectors. Briefly, 293T cells were cotransfected with the IRF-1-expressing plasmid pTRIP.CMV.IVSb.IRF-1.ires.TagRFP, HIV-1 gag-pol, and vesicular stomatitis virus G protein (VSV-G) (at a ratio of 1:0.8:0.2) in Opti-MEM using polyethyleneimine (PEI). After 6 h of transfection, the cells were gently washed once with PBS and refreshed with growth medium. After 48 and 72 h of transfection, the lentivirus-containing supernatants were pooled and filtered through a 0.45-μm-pore-size filter. Two hours of ultracentrifugation (22,000 rpm) was used to concentrate lentiviral particles. The pellet was subsequently resuspended and stored at −80°C at a dilution of 7 log viral RNA copies per ml.

For the transduction assay, HG23 cells were seeded into a 48-well plate (5×10^4 cells per well) and transduced with lentiviral pseudoparticles encoding IRF-1. After 2 days of culture, the cells were collected for detection of IRF-1 by qRT-PCR and Western blotting.

STAT1 knockout in Huh7 cells using the CRISPR/Cas9 system. A STAT1 KO Huh7 clone was established with a Lenti-CRISPR/Cas9 system (STAT1 single-guide RNA [sgRNA], TCCCATTACAGGCTCAG TCG). In brief, HEK293T cells were cotransfected with lentiCRISPRv2-STAT1, pVSVg, and psPAX2 (at a ratio of 1:0.5:0.75) using Fugen HD transfection reagent (Qiagen) according to the manufacturer's instructions. After 24 h of incubation, the medium was replaced with fresh medium supplemented with 1% FCS. Lentivirus-containing supernatants were pooled at 24 and 48 h and subsequently filtered through a 0.45-μm-pore-size filter. Huh7 cells were infected with the lentiviral supernatant for 2 days and further incubated with selection medium containing 4 μg/ml puromycin for 7 days. To obtain knockout clones,

single cells were sorted into 96-well plates and cultured with puromycin (4 μg/ml). The medium was refreshed every 4 days during selection. Cell colonies were collected and identified by Western blotting and genome sequence.

Western blotting. Cell samples were lysed and loaded onto a 10% to 15% sodium dodecyl sulfate-polyacrylamide gel electrophoresis (SDS-PAGE) gel. After electrophoresis at 120 V for 100 min, the proteins were electrotransferred to a polyvinylidene difluoride (PVDF) membrane (Invitrogen) for 1.5 h with an electric current of 250 mA. The membrane was probed with primary antibody plus secondary antibody and detected with an Odyssey 3.0 infrared imaging system (Li-Cor Biosciences). β-Actin was used for standardization of sample loading.

qRT-PCR. Total RNA was isolated with a Macherey NucleoSpin RNA II kit (Bioke, Leiden, Netherlands) and measured with a Nanodrop ND-1000 (Wilmington, DE, USA). cDNA was reverse transcribed from 500 ng RNA using a cDNA synthesis kit (TaKaRa Bio Inc.). The cDNA of a targeted gene transcript was amplified for 50 cycles and quantified with a SYBR Green-based real-time PCR (Applied Biosystems), according to the manufacturer's instructions. All the PCRs were performed in duplicate, and the amplification specificity was confirmed by melting-curve analysis. Human and feline GAPDH genes were used as reference genes. The relative expression of targeted genes was calculated as $2^{-\Delta\Delta CT}$, where $\Delta\Delta C_T$ is equal to $\Delta C_{T\text{sample}}$ minus $\Delta C_{T\text{control}}$ ($\Delta C_T = C_{T[\text{targeted gene}]} - C_{T[\text{GAPDH}]}$). All the primer combinations are listed in the supplemental material.

Statistics. Data are presented as means and standard errors of the mean (SEM). Comparisons between groups were performed with Mann-Whitney tests using GraphPad Prism 5.0 (GraphPad Software Inc., La Jolla, CA, USA). Differences were considered significant at a P value of less than 0.05.

SUPPLEMENTAL MATERIAL

Supplemental material for this article may be found at https://doi.org/10.1128/AAC.00707-18.

SUPPLEMENTAL FILE 1, PDF file, 1.4 MB.

ACKNOWLEDGMENTS

We gratefully acknowledge Erwin Duizer (National Institute for Public Health and the Environment, Bilthoven, Netherlands) for providing the FeCV and CRFK cells. We also thank Charles M. Rice (Rockefeller University, New York, NY, USA) for generously providing the overexpressing lentiviral vector.

This work was supported by the Dutch Digestive Foundation (MLDS) with a career development grant (CDG 1304), by a KWF (Dutch Cancer Society) Young Investigator grant (no. 10140 to Q. Pan), and by the China Scholarship Council (by funding Ph.D. fellowships for W. Dang [201406180072], L. Xu [201306300027], B. Ma [201508330291], Y. Yin [201307720045], and S. Chen [201606760056]).

REFERENCES

1. Bartsch SM, Lopman BA, Ozawa S, Hall AJ, Lee BY. 2016. Global economic burden of norovirus gastroenteritis. PLoS One 11:e0151219. https://doi.org/10.1371/journal.pone.0151219.
2. Ye X, Van JN, Munoz FM, Revell PA, Kozinetz CA, Krance RA, Atmar RL, Estes MK, Koo HL. 2015. Noroviruses as a cause of diarrhea in immunocompromised pediatric hematopoietic stem cell and solid organ transplant recipients. Am J Transplant 15:1874–1881. https://doi.org/10.1111/ajt.13227.
3. Kaufman SS, Chatterjee NK, Fuschino ME, Morse DL, Morotti RA, Magid MS, Gondolesi GE, Florman SS, Fishbein TM. 2005. Characteristics of human calicivirus enteritis in intestinal transplant recipients. J Pediatr Gastroenterol Nutr 40:328–333. https://doi.org/10.1097/01.MPG.0000155182.54001.48.
4. Schwartz S, Vergoulidou M, Schreier E, Loddenkemper C, Reinwald M, Schmidt-Hieber M, Flegel WA, Thiel E, Schneider T. 2011. Norovirus gastroenteritis causes severe and lethal complications after chemotherapy and hematopoietic stem cell transplantation. Blood 117:5850–5856. https://doi.org/10.1182/blood-2010-12-325886.
5. Morris J, Morris C. 2015. Nitazoxanide is effective therapy for norovirus gastroenteritis after chemotherapy and hematopoietic stem cell transplantation (HSCT). Biol Blood Marrow Transplant 21:S255–S256.
6. Stockis A, De Bruyn S, Gengler C, Rosillon D. 2002. Nitazoxanide pharmacokinetics and tolerability in man during 7 days dosing with 0.5 g and 1 g b.i.d. Int J Clin Pharmacol Ther 40:221–227. https://doi.org/10.5414/CPP40221.
7. Rossignol JF. 2014. Nitazoxanide: a first-in-class broad-spectrum antiviral agent. Antiviral Res 110:94–103. https://doi.org/10.1016/j.antiviral.2014.07.014.
8. La Frazia S, Ciucci A, Arnoldi F, Coira M, Gianferretti P, Angelini M, Belardo G, Burrone OR, Rossignol JF, Santoro MG. 2013. Thiazolides, a new class of antiviral agents effective against rotavirus infection, target viral morphogenesis, inhibiting viroplasm formation. J Virol 87:11096–11106. https://doi.org/10.1128/JVI.01213-13.
9. Rossignol JF, La Frazia S, Chiappa L, Ciucci A, Santoro MG. 2009. Thiazolides, a new class of anti-influenza molecules targeting viral hemagglutinin at the post-translational level. J Biol Chem 284:29798–29808. https://doi.org/10.1074/jbc.M109.029470.
10. Elazar M, Liu M, McKenna SA, Liu P, Gehrig EA, Puglisi JD, Rossignol JF, Glenn JS. 2009. The anti-hepatitis C agent nitazoxanide induces phosphorylation of eukaryotic initiation factor 2alpha via protein kinase activated by double-stranded RNA activation. Gastroenterology 137:1827–1835. https://doi.org/10.1053/j.gastro.2009.07.056.
11. Trabattoni D, Gnudi F, Ibba SV, Saulle I, Agostini S, Masetti M, Biasin M, Rossignol JF, Clerici M. 2016. Thiazolides elicit anti-viral innate immunity and reduce HIV replication. Sci Rep 6:27148. https://doi.org/10.1038/srep27148.
12. Rossignol JF, Abu-Zekry M, Hussein A, Santoro MG. 2006. Effect of nitazoxanide for treatment of severe rotavirus diarrhoea: randomised double-blind placebo-controlled trial. Lancet 368:124–129. https://doi.org/10.1016/S0140-6736(06)68852-1.
13. Gorgeis J, Sizemore C, Bashey A, Holland HK, Solomon SR, Morris LE, Solh M. 2017. Nitazoxanide is effective therapy for norovirus gastroenteritis after hematopoietic stem cell transplantation. Biol Blood Marrow Transplant 23:S197–S198.
14. Dang W, Yin Y, Peppelenbosch MP, Pan Q. 2017. Opposing effects of

nitazoxanide on murine and human norovirus. J Infect Dis 216:780–782. https://doi.org/10.1093/infdis/jix377.
15. Woodward J, Gkrania-Klotsas E, Kumararatne D. 2017. Chronic norovirus infection and common variable immunodeficiency. Clin Exp Immunol 188:363–370. https://doi.org/10.1111/cei.12884.
16. Wang W, Xu L, Su J, Peppelenbosch MP, Pan Q. 2017. Transcriptional regulation of antiviral interferon-stimulated genes. Trends Microbiol 25:573–584. https://doi.org/10.1016/j.tim.2017.01.001.
17. Xu L, Wang W, Peppelenbosch MP, Pan Q. 2017. Noncanonical Antiviral Mechanisms of ISGs: Dispensability of Inducible Interferons. Trends Immunol 38:1–2. https://doi.org/10.1016/j.it.2016.11.002.
18. Schoggins JW, Wilson SJ, Panis M, Murphy MY, Jones CT, Bieniasz P, Rice CM. 2011. A diverse range of gene products are effectors of the type I interferon antiviral response. Nature 472:481–485. https://doi.org/10.1038/nature09907.
19. Schoggins JW, MacDuff DA, Imanaka N, Gainey MD, Shrestha B, Eitson JL, Mar KB, Richardson RB, Ratushny AV, Litvak V, Dabelic R, Manicassamy B, Aitchison JD, Aderem A, Elliott RM, Garcia-Sastre A, Racaniello V, Snijder EJ, Yokoyama WM, Diamond MS, Virgin HW, Rice CM. 2014. Pan-viral specificity of IFN-induced genes reveals new roles for cGAS in innate immunity. Nature 505:691–695. https://doi.org/10.1038/nature12862.
20. Wang W, Xu L, Brandsma JH, Wang Y, Hakim MS, Zhou X, Yin Y, Fuhler GM, van der Laan LJ, van der Woude CJ, Sprengers D, Metselaar HJ, Smits R, Poot RA, Peppelenbosch MP, Pan Q. 2016. Convergent transcription of interferon-stimulated genes by TNF-alpha and IFN-alpha augments antiviral activity against HCV and HEV. Sci Rep 6:25482. https://doi.org/10.1038/srep25482.
21. Bines JE, Danchin M, Jackson P, Handley A, Watts E, Lee KJ, West A, Cowley D, Chen MY, Barnes GL, Justice F, Buttery JP, Carlin JB, Bishop RF, Taylor B, Kirkwood CD, RV3 Rotavirus Vaccine Program. 2015. Safety and immunogenicity of RV3-BB human neonatal rotavirus vaccine administered at birth or in infancy: a randomised, double-blind, placebo-controlled trial. Lancet Infect Dis 15:1389–1397. https://doi.org/10.1016/S1473-3099(15)00227-3.
22. van Beek J, van der Eijk AA, Fraaij PL, Caliskan K, Cransberg K, Dalinghaus M, Hoek RA, Metselaar HJ, Roodnat J, Vennema H, Koopmans MP. 2017. Chronic norovirus infection among solid organ recipients in a tertiary care hospital, the Netherlands, 2006-2014. Clin Microbiol Infect 23:265.e269-265.e213. https://doi.org/10.1016/j.cmi.2016.12.010.
23. Florescu DF, Hermsen ED, Kwon JY, Gumeel D, Grant WJ, Mercer DF, Kalil AC. 2011. Is there a role for oral human immunoglobulin in the treatment for norovirus enteritis in immunocompromised patients? Pediatr Transplant 15:718–721. https://doi.org/10.1111/j.1399-3046.2011.01556.x.
24. Woodward JM, Gkrania-Klotsas E, Cordero-Ng AY, Aravinthan A, Bandoh BN, Liu H, Davies S, Zhang H, Stevenson P, Curran MD, Kumararatne D. 2015. The role of chronic norovirus infection in the enteropathy associated with common variable immunodeficiency. Am J Gastroenterol 110:320–327. https://doi.org/10.1038/ajg.2014.432.
25. Chang KO, Sosnovtsev SV, Belliot G, King AD, Green KY. 2006. Stable expression of a Norwalk virus RNA replicon in a human hepatoma cell line. Virology 353:463–473. https://doi.org/10.1016/j.virol.2006.06.006.
26. Atmar RL, Opekun AR, Gilger MA, Estes MK, Crawford SE, Neill FH, Graham DY. 2008. Norwalk virus shedding after experimental human infection. Emerg Infect Dis 14:1553–1557. https://doi.org/10.3201/eid1410.080117.
27. Wobus CE, Thackray LB, Virgin HWT. 2006. Murine norovirus: a model system to study norovirus biology and pathogenesis. J Virol 80:5104–5112. https://doi.org/10.1128/JVI.02346-05.
28. Nims R, Plavsic M. 2013. Inactivation of caliciviruses. Pharmaceuticals 6:358–392. https://doi.org/10.3390/ph6030358.
29. McCann KB, Lee A, Wan J, Roginski H, Coventry MJ. 2003. The effect of bovine lactoferrin and lactoferricin B on the ability of feline calicivirus (a norovirus surrogate) and poliovirus to infect cell cultures. J Appl Microbiol 95:1026–1033. https://doi.org/10.1046/j.1365-2672.2003.02071.x.
30. Slomka MJ, Appleton H. 1998. Feline calicivirus as a model system for heat inactivation studies of small round structured viruses in shellfish. Epidemiol Infect 121:401–407. https://doi.org/10.1017/S0950268898001290.
31. Rodriguez MR, Monte K, Thackray LB, Lenschow DJ. 2014. ISG15 functions as an interferon-mediated antiviral effector early in the murine norovirus life cycle. J Virol 88:9277–9286. https://doi.org/10.1128/JVI.01422-14.
32. McCartney SA, Thackray LB, Gitlin L, Gilfillan S, Virgin HW, Colonna M. 2008. MDA-5 recognition of a murine norovirus. PLoS Pathog 4:e1000108. https://doi.org/10.1371/journal.ppat.1000108.
33. Changotra H, Jia Y, Moore TN, Liu G, Kahan SM, Sosnovtsev SV, Karst SM. 2009. Type I and type II interferons inhibit the translation of murine norovirus proteins. J Virol 83:5683–5692. https://doi.org/10.1128/JVI.00231-09.
34. Miyamoto M, Fujita T, Kimura Y, Maruyama M, Harada H, Sudo Y, Miyata T, Taniguchi T. 1988. Regulated expression of a gene encoding a nuclear factor, IRF-1, that specifically binds to IFN-beta gene regulatory elements. Cell 54:903–913. https://doi.org/10.1016/S0092-8674(88)91307-4.
35. Fujita T, Reis LF, Watanabe N, Kimura Y, Taniguchi T, Vilcek J. 1989. Induction of the transcription factor IRF-1 and interferon-beta mRNAs by cytokines and activators of second-messenger pathways. Proc Natl Acad Sci U S A 86:9936–9940. https://doi.org/10.1073/pnas.86.24.9936.
36. Xu L, Zhou X, Wang W, Wang Y, Yin Y, Laan LJ, Sprengers D, Metselaar HJ, Peppelenbosch MP, Pan Q. 2016. IFN regulatory factor 1 restricts hepatitis E virus replication by activating STAT1 to induce antiviral IFN-stimulated genes. FASEB J 30:3352–3367. https://doi.org/10.1096/fj.201600356R.
37. Hu S, Xie Z, Onishi A, Yu X, Jiang L, Lin J, Rho HS, Woodard C, Wang H, Jeong JS, Long S, He X, Wade H, Blackshaw S, Qian J, Zhu H. 2009. Profiling the human protein-DNA interactome reveals ERK2 as a transcriptional repressor of interferon signaling. Cell 139:610–622. https://doi.org/10.1016/j.cell.2009.08.037.
38. Di Santo N, Ehrisman J. 2014. A functional perspective of nitazoxanide as a potential anticancer drug. Mutat Res 768:16–21. https://doi.org/10.1016/j.mrfmmm.2014.05.005.
39. Rossignol JF, El-Gohary YM. 2006. Nitazoxanide in the treatment of viral gastroenteritis: a randomized double-blind placebo-controlled clinical trial. Aliment Pharmacol Ther 24:1423–1430. https://doi.org/10.1111/j.1365-2036.2006.03128.x.
40. Rossignol JF, Lopez-Chegne N, Julcamoro LM, Carrion ME, Bardin MC. 2012. Nitazoxanide for the empiric treatment of pediatric infectious diarrhea. Trans R Soc Trop Med Hyg 106:167–173. https://doi.org/10.1016/j.trstmh.2011.11.007.
41. Siddiq DM, Koo HL, Adachi JA, Viola GM. 2011. Norovirus gastroenteritis successfully treated with nitazoxanide. J Infect 63:394–397. https://doi.org/10.1016/j.jinf.2011.08.002.
42. Kempf B, Edgar JD, McCaughey C, Devlin LA. 2017. Nitazoxanide is an ineffective treatment of chronic norovirus in patients with X-linked agammaglobulinemia and may yield false-negative polymerase chain reaction findings in stool specimens. J Infect Dis 215:486–487. https://doi.org/10.1093/infdis/jiw497.
43. Dang W, Yin Y, Wang Y, Wang W, Su J, Sprengers D, van der Laan LJW, Felczak K, Pankiewicz KW, Chang KO, Koopmans MPG, Metselaar HJ, Peppelenbosch MP, Pan Q. 2017. Inhibition of calcineurin or IMP dehydrogenase exerts moderate to potent antiviral activity against norovirus replication. Antimicrob Agents Chemother 61:e01095-17. https://doi.org/10.1128/AAC.01095-17.
44. Thomas E, Feld JJ, Li Q, Hu Z, Fried MW, Liang TJ. 2011. Ribavirin potentiates interferon action by augmenting interferon-stimulated gene induction in hepatitis C virus cell culture models. Hepatology 53:32–41. https://doi.org/10.1002/hep.23985.
45. Duizer E, Bijkerk P, Rockx B, De Groot A, Twisk F, Koopmans M. 2004. Inactivation of caliciviruses. Appl Environ Microbiol 70:4538–4543. https://doi.org/10.1128/AEM.70.8.4538-4543.2004.
46. Yin Y, Bijvelds M, Dang W, Xu L, van der Eijk AA, Knipping K, Tuysuz N, Dekkers JF, Wang Y, de Jonge J, Sprengers D, van der Laan LJ, Beekman JM, Ten Berge D, Metselaar HJ, de Jonge H, Koopmans MP, Peppelenbosch MP, Pan Q. 2015. Modeling rotavirus infection and antiviral therapy using primary intestinal organoids. Antiviral Res 123:120–131. https://doi.org/10.1016/j.antiviral.2015.09.010.
47. Dang W, Xu L, Yin Y, Chen S, Wang W, Hakim MS, Chang KO, Peppelenbosch MP, Pan Q. 2018. IRF-1, RIG-I and MDA5 display potent antiviral activities against norovirus coordinately induced by different types of interferons. Antiviral Res 155:48–59. https://doi.org/10.1016/j.antiviral.2018.05.004.
48. Bidawid S, Malik N, Adegbunrin O, Sattar SA, Farber JM. 2003. A feline kidney cell line-based plaque assay for feline calicivirus, a surrogate for Norwalk virus. J Virol Methods 107:163–167. https://doi.org/10.1016/S0166-0934(02)00214-8.
49. Ettayebi K, Crawford SE, Murakami K, Broughman JR, Karandikar U, Tenge VR, Neill FH, Blutt SE, Zeng XL, Qu L, Kou B, Opekun AR, Burrin D, Graham DY, Ramani S, Atmar RL, Estes MK. 2016. Replication of human noroviruses in stem cell-derived human enteroids. Science 353:1387–1393. https://doi.org/10.1126/science.aaf5211.